

# Tomographic background-oriented schlieren techniques for three-dimensional density field reconstruction in shock-containing flows.

R. Kirby<sup>1</sup>, D. J. Tan<sup>1</sup>, C. Atkinson<sup>1</sup>, D. Edgington-Mitchell<sup>1</sup>

<sup>1</sup>Laboratory for Turbulence Research in Aerospace and Combustion,  
Department of Mechanical and Aerospace Engineering  
Monash University, Victoria, 3800, Australia

## Abstract

Two measurement techniques for acquiring pixel displacement data for tomographic background oriented schlieren are compared; the first analyses image pairs of an optimised random-dot pattern using a conventional cross-correlation algorithm. The second evaluates optical flow displacements for image pairs of a fractal texture background composed of multi-scale wavelet noise. Quasi-3D tomographic reconstruction is performed under the parallel-ray assumption using an algebraic method, initialised with large-gradient regions from a filtered back-projection gradient inversion, for improved clarity and noise reduction. Reconstruction of the near-field density of a highly underexpanded jet from an elliptical nozzle of aspect ratio 2:1 is performed using both optical flow and cross-correlation displacement fields. Diffraction effects at the Mack disk are seen to produce strong artefacts in reconstructed gradient fields. Differences in gradient components from optical flow and cross-correlation are effectively smoothed by Poisson integration, yielding similar final density distributions, stressing that selection of a suitably accurate method for integration of the Poisson equation is required to preserve increased fidelity of gradient fields. Good qualitative agreement in shock structure is found with respect to existing studies.

## 1 Introduction

The inherent complexity of compressible, shock-containing, flows demands three-dimensional visualisation methods, while requiring non-intrusive imaging. The ability to quantify the effect of density gradients on the path of light through an inhomogeneous flow field, more traditionally visualised using schlieren methods at the cost of line-of-sight ambiguity, has encouraged the adoption of the background-oriented schlieren (BOS) method. BOS provides quantifiable path-integrated light ray deflections  $\epsilon$ , for gradient components local to the ray trajectory  $\mathbf{p}$ ,

$$\epsilon = \frac{G}{n_0} \int_{\mathbf{p}} \nabla \rho(\xi) d\xi \quad (1)$$

where the above relies on the simple relationship between density and refractive index  $n$  for a gas [1], given by the linear Gladstone-Dale relation, under the assumption of constant wavelength illumination

$$\rho(x, t)G(\lambda) = n(x, t) - 1 \quad (2)$$

for  $G$  the Gladstone-Dale constant. Recovery of the spatial density field  $\rho(\mathbf{x})$  requires inversion of (1) based on knowledge of numerous deflections  $\epsilon$ . Ray deflections are inferable through background displacements  $\Delta \mathbf{x}_p$ , quantifying the optical distortion between reference and refracted image pairs taken in absence of, or through, the flow object in turn. Displacement vectors may be evaluated using cross-correlation algorithms typically used in PIV applications [2], or by computing the optical flow between image pairs [3]. Net deflection angles may be related to pixel displacements occurring between reference and displaced image pairs assuming paraxial rays, and under the small-angle approximation, using setup geometry and image magnification [1].

Experimentally derived BOS deflections may be passed through conventional Fourier-based algorithms under the refractionless ray assumption, for rapid reconstruction and resolution of steep gradients. Recovered gradient fields may then be numerically integrated to form the source term for the Poisson equation, the solution to which returns the spatial refractive index field. Streak artefacts are manifest in filtered back-projection (FBP) methods, particularly when limited to few viewing angles. At the cost of clarity and ease of implementation, artefacts may largely be avoided by using an algebraic reconstruction technique (ART), in place of FBP, to recover the components of the refractive index gradient. The algebraic approach may be combined with a ray tracing procedure, which allows the straight ray assumption to be relaxed if refractive effects are considered non-negligible, or setup dimensions invalidate the parallel-ray simplification [4]. The error resulting from the application of conventional inversion algorithms, under the assumption of non-refracting rays, may be significant for strongly refracting fields.

Early applications of BOS have considered two-dimensional (2D) planar flows, thereby removing the transverse (line-of-sight) density gradient [5]. Studies of three-dimensional (3D) problems predominantly consider time-averaged axisymmetric mean fields, enabling direct tomographic reconstruction using average displacement fields from a single viewpoint, via well-known inverse Radon methods under radial symmetry [6]. Algebraic reconstruction techniques (ART) have been applied successfully in tandem with ray tracing procedures, for non-axisymmetric and time resolved flows, utilising large camera arrays [4] or under assumptions of rotational symmetry [7].

While basic algebraic methods are known to behave robustly when provided with limited data, challenges include poor resolution of steep gradients, and the subsequent loss of clarity in the final Poisson integrated refractive index field. Solutions are also sensitive to initial conditions. Hartmann & Seume [8] and Atkinson [9] report notable improvement through

---

Corresponding author.  
E-mail address: rkkir1@student.monash.edu

initialisation of ART with a subset of the gradient field extracted from an initial FBP reconstruction.

In this paper the sensitivity of the reconstructed density field to the input displacement field is tested experimentally. Two approaches to extracting the ray displacements are compared, as detailed in the following section. A shock-containing supersonic elliptical jet is used as a case study. Elliptical jets are of interest due to their mixing [10] and aeroacoustic properties [11], as is well summarized in Gutmark [12]. Supersonic elliptical jets operating in the underexpanded regime exhibit complex shock structures in the potential core [13], that remain poorly understood [14].

## 2 Experimental methodology

Inversion of (1) is based on two-dimensional projection data, acquired in practice from a limited number of viewing angles. BOS measurements are performed in the LTRAC supersonic jet facility. The reader is referred to Tan *et al.* [6] for details of the BOS optical layout and lighting, and related nomenclature. A highly underexpanded jet issuing from an elliptical nozzle of aspect ratio 2:1 serves as the base flow for comparison of measurement techniques. Description of the facility and nozzle geometry may be found in Edgington-Mitchell *et al.* [11]. Experimental parameters are summarised in Table 1, with Reynolds number  $Re$  based on the ideally expanded Mach number at a nozzle pressure ratio (NPR) of 4.2. Images are acquired using a PCO4000 camera, with CCD array of 4008x2672 pixels, of size  $9\mu\text{m}/\text{px}$ , and a 105mm AF Micro Nikkor lens. An f-stop of 22 is used for maximum depth-of-field. Each image is exposed for  $95\mu\text{s}$ , despite the characteristic timescales of the flow being typically much shorter. This is done to maximize signal to noise ratio in the image, and since the inability to resolve fine-scale turbulence is irrelevant when only the mean displacements will be used in the computation of gradient components. Reference background images are acquired prior to displaced images for each viewing angle. Two hundred samples are acquired during a single run for time-averaging. Each mean field is mirrored across a single axis under the assumption of quarter-symmetry, providing 20 viewing angles about the major axis half-circle.

### 2.1 BOS displacements

Two data sets of the same base flow, each at 10 viewing angles, are obtained; the first using a random-dot BOS background pattern designed according to optimal PIV seeding parameters unique to the optical layout [15]. The seeding density is estimated to be approximately 4.85 particles per  $16\times 16$  pixel window. The full background contains 220000 particles of size  $70\mu\text{m}$ . A 21mm sample is enlarged in Fig. 1a. Multigrid cross-correlation is performed using PIVview 2C in Speckle Displacement mode for evaluation of pixel displacement vectors between every displaced image and a single reference image at each view, using a final interrogation window of size  $16\times 16$  with an overlap of 50%. A  $3\times 3$  pixel median filter is applied across each snapshot, prior to time-averaging at each viewing angle.

Data acquisition is repeated using a fractal texture background composed of multi-scale wavelet noise, for the purposes of optical flow evaluation. A 21mm sample is shown in Fig. 1b. Generation of wavelet noise functions is described in detail by Cook & DeRose [16]. Practical implementation in BOS is discussed by Atcheson, Heidrich & Ihrke [17], who find that wavelet noise backgrounds are able to provide greater accuracy, particularly when combined with multi-scale gradient-based optical flow algorithms [18]. A major advantage of optical flow

is the potential to provide dense fields at one vector per image pixel. In this case fields are downsampled to match those obtained via PIVview. No filtering is applied, which results in slightly noisier gradient fields – an example is provided in Fig. 3.

Experimental Parameters	
$Z_B$ (mm)	562
$Z_D$ (mm)	206
$f$ (mm)	105
Spatial Resolution ( $\mu\text{m}/\text{px}$ )	39.2
D (mm)	14.1
$\rho_0$ ( $\text{kg}/\text{m}^3$ )	1.22
$Re$	$8.74\times 10^5$
NPR	4.2

Table 1: Experimental BOS layout and flow parameters.

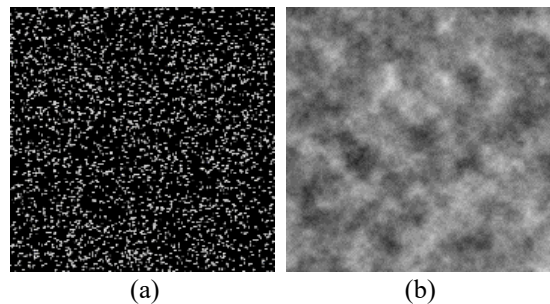


Figure 1: 21mm background samples for (a) random-dot and (b) wavelet noise.

### 2.2 Tomographic reconstruction

Similar to the approach of Venkatakrishnan & Meier [5] FBP is performed on deflection data, using Shepp-Logan frequency domain filtering for attenuation of high-frequency noise. A subset of the gradient field obtained using FBP is then passed to a simultaneous ART (SART) scheme for resolution of steep gradients and reduction of artefacts, following improvements seen by Hartmann & Seume [8] and Atkinson [9].

A masking procedure is used to extract high-gradient regions, assumed to be confined within a variable ellipse whose semi-major and semi-minor axes are defined by the extent of the shear layer along the respective axes. Sobel edge detection is used to identify the outer edge of the shear layer. A threshold is placed over the gradient magnitude to remove low gradients within the flow domain. The relative success of masking is found to be highly sensitive to the structure of the gradient field, and is hence difficult to optimise a priori without knowledge of artefact-free characteristics. For instance, flow features of interest may be removed by placing a threshold on gradient magnitude, which may preserve high-intensity artefacts. Over-thresholding may mitigate any improvement over a homogeneous initial condition, presenting a difficulty in automation further to the uniqueness of each image in scale and intensity.

Iterative SART is performed using AIR Tools MATLAB Package [19], under the assumption of parallel beam tomography. Each axial plane is reconstructed independently. Discrete second-order approximations to the derivative terms are combined to estimate the source term for the 2D Poisson equation. A second-order (5-point) discretisation of the Poisson

equation is solved using an iterative SOR scheme. The convergence tolerance is set to a maximum difference of  $10^{-10}$  in successive values of  $n$  at any point. Each plane is solved independently, enforcing ambient Dirichlet boundary conditions over a square domain. The computational cost of Poisson integration may be relieved by reduction of the domain size, as performed in 3D by Atcheson *et al.* [4] through the definition of a visual hull. Noise levels in the resultant solution are also reduced by the consequent elimination of far-field artefacts in recovered gradients, prior to computation of the Poisson source field. In this case, the domain is cropped prior to gradient reconstruction.

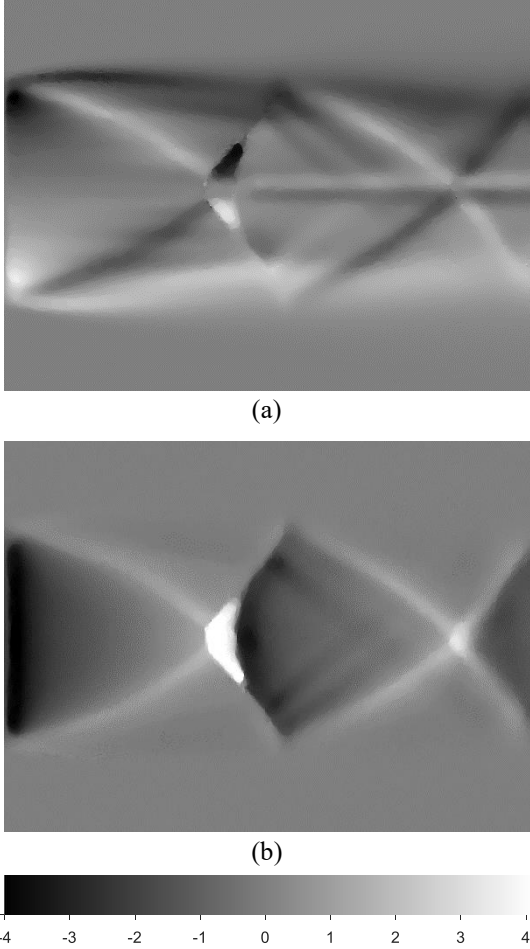


Figure 2: Example time-averaged pixel displacements viewed along the minor axis, obtained using optical flow algorithm (a)  $\Delta y$  (b)  $\Delta x$  in pixels.

### 3 Results

#### 3.1 Recovery of spatial gradient components

Gradients are recovered from a single displacement field component,  $\Delta y$ , assuming independent parallel-ray projections at each downstream plane. Reconstructed components at a single plane, immediately upstream of the Mach disk, are compared in Fig. 3. This plane is chosen to highlight the dominance of artefacts surrounding the Mach disk and reflected oblique shock, particularly evident using the downsampled optical flow data (Fig. 3a-b). Spatial filtering performed on cross-correlation data is observed to provide smoother fields without significant loss of clarity (Fig. 3c-d).

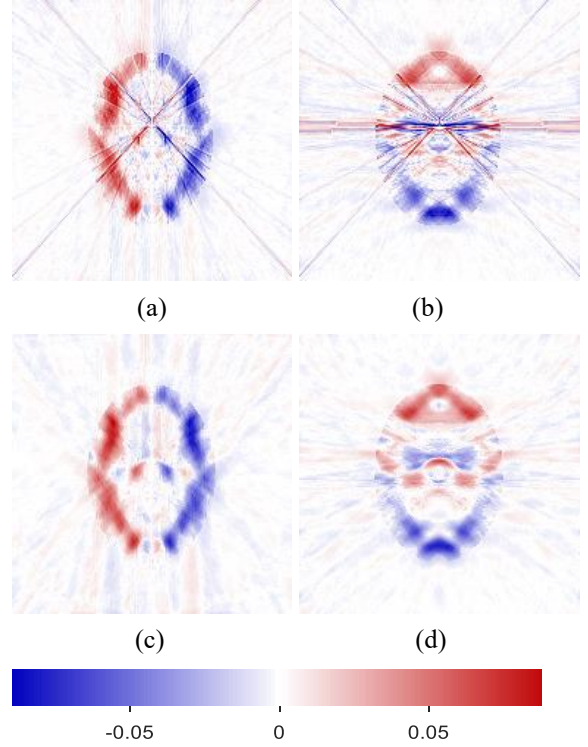


Figure 3: Reconstructed gradient components (scaled by inverse step size) at plane 94 ( $x/D = 1.04$ ) using optical flow displacements (a)  $\partial n / \partial x$  (b)  $\partial n / \partial y$  and cross-correlation data (c)  $\partial n / \partial x$  (d)  $\partial n / \partial y$ .

#### 3.2 Quantitative near-field density

Normalised density distributions for the minor-axis and major-axis planes are shown in Fig. 4. Results are almost indistinguishable for optical flow and cross-correlation methods, so only the former is shown. Figure 5 compares axial distributions for arbitrary locations, illustrating variable agreement in cross-correlated and optical flow fields. Fine-scale features appear to be better resolved using optical flow in some locations.

Good qualitative agreement is observed in relation to PIV velocity distributions at the same flow conditions [10]. A low density shear layer originating behind the Mach disk is observed to persist past the second shock cell, as observed in corresponding high-resolution schlieren images [11]. In comparison with numerical shock structures found at lower NPR by Menon & Skews [13], it is noted that the first axis-switching event is not complete by the second shock reflection. The first shock cell appears to share similarities with numerical results of Li *et al.* [14] for both elliptical and rectangular nozzle geometries at higher NPR, suggesting that even slight asymmetries present in real flows may result in significant changes in shock structure, including the formation of ‘corner’ shocks in regions of locally high curvature.

Artefacts in the reconstructed density field are evident at the axial location of the Mach disk. This is almost certainly due to diffraction effects at the Mach disk itself. A strong shock oriented at a grazing angle to the direction of light propagation has been observed to diffract the incident light in both PIV [20] and PLIF [21] applications. Typically, this diffraction only influences the measurement once the light propagates past the shock-wave, but the path-integrated nature of BOS (and the present symmetry assumptions) result in errors in the density field through the entire radial extent of the jet in the vicinity of the Mach disk.

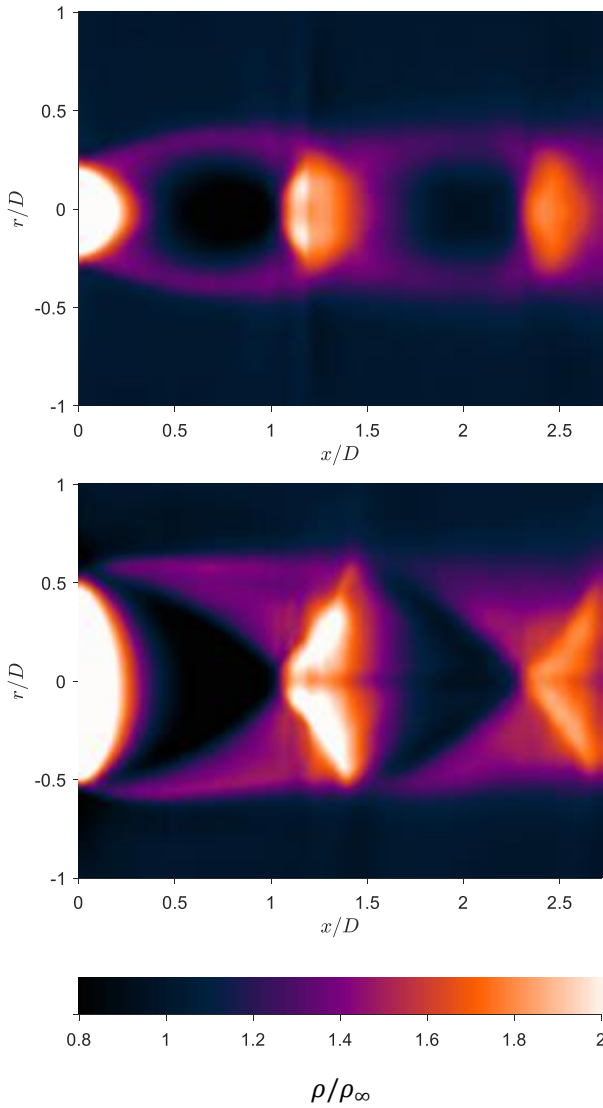


Figure 4: Major-axis plane, minor-axis plane normalised density field reconstructions obtained using optical flow displacements.

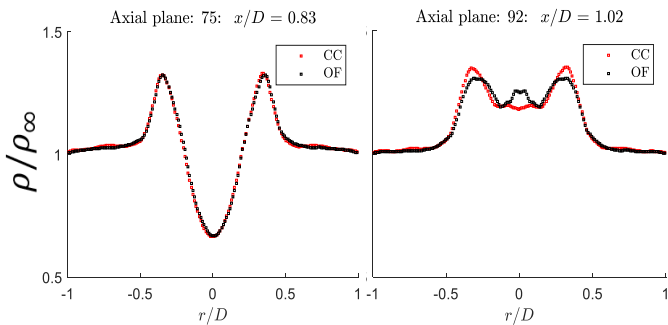


Figure 5: Transverse density distribution along the minor axis (symmetry) for axial planes 75 & 92.

## 4 Conclusions

The ability of several approaches to tomographic background-oriented schlieren have been tested, comparing their ability to resolve the density field of a highly underexpanded elliptical supersonic jet. The optical-flow based approach proved significantly more susceptible to diffraction effects at the edge of strong shock-waves, as well as being generally noisier. Despite this, the reconstructed density fields using the two approaches were almost identical, indicating that the method of solution for the Poisson integration may be a more important factor than the choice of method for extracting displacements

from the distorted background pattern.

## 5 Acknowledgment

The authors gratefully acknowledge the assistance of T. Knast in improving the robustness of the imaging setup.

## References

- [1] H. Richard, M. Raffel, Meas. Sci. Technol. 12 (9) (2001) 1576-1585.
- [2] J. Soria, Exp. Therm. Fluid Sci. 12 (2) (1996) 221-233.
- [3] G. Settles, M.J. Hargather, Meas. Sci. Technol. 28 (4) (2017) 042001.
- [4] B. Atcheson, I. Ihrke, W. Heidrich, A. Tevs, D. Bradley, M. Magnor, H. Seidel, ACM Trans. Graph. 27 (5) (2008) 132.
- [5] L. Venkatakrishnan, G.E.A. Meier, Exp. Fluids. 37 (2) (2004) 237-347.
- [6] D.J. Tan, D. Edgington-Mitchell, D. Honnery, Exp. Fluids 56 (11) (2015) 204.
- [7] H.M. Lang, K. Oberleithner, C.O. Paschereit, M. Seiber, Exp. Fluids 58 (7) 88.
- [8] U. Hartmann, J.R. Seume, Meas. Sci. Technol. 27 (9) (2016) 097001.
- [9] C. Atkinson, S. Amjad, J. Soria, A Tomographic Background-Oriented Schlieren Method for 3D Density Field Measurements in Heated Jets. In 11<sup>th</sup> Asia-Pacific Conference on Combustion, 2017.
- [10] D.M. Mitchell, D.R. Honnery, J. Soria, Exp. Fluids 54 (7) (2013) 1578.
- [11] D. Edgington-Mitchell, D. Honnery, J. Soria, International Journal of Aeroacoustics, 14 (7), (2015) 1005-1024.
- [12] E.J. Gutmark, F.F. Grinstein, Annu. Rev. Fluid Mech. 31 (1) (1999) 239-272.
- [13] N. Menon, B.W. Skews, Shock Waves 20 (2010) 175-190.
- [14] X. Li, R. Zhou, W. Yao, X. Fan, Appl. Therm. Eng. 125 (2017) 240-253.
- [15] M. Raffel, C. Willert, J. Kompenhans, Particle image velocimetry: a practical guide, Springer, Berlin, 1998
- [16] R.L. Cook, T. DeRose, ACM Trans Graph 24 (3) (2005) 803-811.
- [17] B. Atcheson, W. Heidrich, I. Ihrke, Exp. Fluids 46 (3) (2009) 467-476.
- [18] C. Liu, *Beyond Pixels: Exploring New Representations and Applications for Motion Analysis*, PhD thesis, Massachusetts Institute of Technology, Massachusetts, USA, 2009.
- [19] P.C. Hansen, M. Saxild-Hansen, J. Comput. Appl Math. 236 (8) (2012) 2167-2178.
- [20] G. Bell, J. Soria, D. Honnery, D. Edgington-Mitchell. Particle Image Velocimetry Analysis of the Twin Supersonic Jet Structure and Standing-Wave. In 23<sup>rd</sup> AIAA/CEAS Aeroacoustics Conference, 2017, 3517.
- [21] J. Yoo, D. Mitchell, D.F. Davidson, R.K. Hanson, Exp. Fluids. 49 (4) (2010), 751-759.